communications physics

ARTICLE

https://doi.org/10.1038/s42005-023-01383-x OPEN

# Tera-sample-per-second arbitrary waveform generation in a synthetic dimension

Yiran Guan [1], Jiejun Zhang [1✉], Lingzhi Li[1], Ruidong Cao[1], Guangying Wang[1], Jingxu Chen[1], Xudong Wang[1], Bai-Ou Guan[1] & Jianping Yao [1,2✉]

Synthetic dimension opens new horizons in quantum physics and topological photonics by enabling new dimensions for field and particle manipulations. The most appealing property of the photonic synthetic dimension is its ability to emulate high-dimensional optical behavior in a unitary physical system. Here we show that the photonic synthetic dimension can transform technical problems in photonic systems between dimensionalities, providing unexpected solutions to technical problems that are otherwise challenging. Specifically, we propose and experimentally demonstrate a fully reconfigurable photonic Galton board (PGB) in the temporal synthetic dimension, in which the temporal high-speed challenge is translated into a spatial fiber-optic length matching problem, leading to the generation of tera-sample-per-second arbitrary waveforms with ultimate flexibility. In the experiments, an arbitrary waveform with a widely tunable sampling rate, ranging from 10.42 GSa/s to a record high of 1.64 TSa/s, is demonstrated. The concept of dimension conversion offers possible solutions to various physical dimension-related problems, such as super-resolution imaging, high-resolution spectroscopy, and high-precision time measurement.

[1] Guangdong Provincial Key Laboratory of Optical Fiber Sensing and Communications, Institute of Photonics Technology, Jinan University, Guangzhou 511443, China. [2] Microwave Photonics Research Laboratory, School of Electrical Engineering and Computer Science, University of Ottawa, Ottawa, ON K1N 6N5, Canada. ✉email: zhangjiejun@jnu.edu.cn; jpyao@uottawa.ca

The synthetic dimension provides additional dimensions for field and particle operations to explore higher dimensional physical phenomena in a lower-dimensional physical system[1,2]. Recently, synthetic dimension has opened a new direction in implementing photonic systems[3,4]. By dynamically modulating optical modes[5–7], orbital angular momenta[8,9], or by using multiple pulses[10–14], a photonic lattice in synthetic space can be constructed. In addition, for a photonic system having multiple optical parameter spaces, each parameter can be seen as an extra synthetic dimension[15,16]. Based on synthetic dimensions, various new photonic systems have been proposed for the demonstration of optical quantum walks[17,18], band structure[5,14], topological photonics[10,19–21], and parity-time symmetry[16,22,23]. In 2020, Szameit et al. presented an efficient funnel for light in temporal synthetic space based on the non-Hermitian skin effect[10], in which the light field travels towards an interface regardless of its shape and input position. On the other hand, the Galton board invented by Galton in 1889 demonstrated the central limit theorem by observing the distribution of beads at the bottom of the board. It has been introduced to the optics community for studying spectral diffusion of a light wave[24] and quantum phenomenon in nonlinear optics[25–27]. The optical funnel is like a special Galton board, in which the drop position of the beads is controlled.

Microwave arbitrary waveforms with a wide bandwidth have been widely used in modern radar and microwave imaging systems to increase the range and imaging resolution[28–31]. Due to the limited sampling rate of an electronic analog-to-digital converter (ADC), a state-of-the-art electronic arbitrary waveform generator (AWG) using an electronic ADC can operate with a sampling rate up to 128 GSa/s and a maximum analog bandwidth of 65 GHz[32]. On the other hand, a photonic-assisted microwave AWG can operate at a speed far beyond 128 GSa/s thanks to the inherent high speed and broad bandwidth offered by modern photonics. In an arbitrary waveform generation system based on optical pulse shaping, a spatial light modulator (SLM)[29,33,34], metasurface[35,36], or other spatial mask[37] is used to shape the optical spectrum of an ultra-short optical pulse, to tailor the magnitude and phase of the spectrum corresponding to the temporal waveform to be generated[38]. However, those optical pulse shaping systems are implemented based on free-space optics, making the systems bulky, costly, and vulnerable to environmental disturbances. In recent years, benefiting from the rapid progress in microwave photonics[39–41], microwave arbitrary waveform generation implemented by fiber-optics[42–49] or photonic integrated devices[50–55] in the temporal[43–46] or frequency domain[47–49,51,53] has been reported. AWGs based on fiber-optics or photonic integrated devices have lower loss, smaller size and better waveform reconfigurability, but the bandwidths of generated microwave waveforms are still small, limited by the bandwidths of electro-optical modulators and photodetectors. Synthetic dimension is one potential technique to address the challenges in arbitrary waveform generation, providing a potential solution to generate arbitrary waveforms at a much higher sampling rate and much wider bandwidth, and at the same time, with full reconfigurability and ultimate flexibility.

Here a photonic Galton board (PGB) in the temporal synthetic dimension is proposed and experimentally demonstrated, in which the temporal high-speed challenge is translated into a spatial fiber-optic length matching problem, leading to the realization of tera-sample-per-second (TSa/s) arbitrary waveform generation with ultimate flexibility. Specifically, the PGB is implemented based on two coupled fiber-optic loops with different time delays, and two acousto-optic modulators (AOMs), with one incorporated in each of the two loops, to control the gain or loss to the optical pulses recirculating in the loop, resulting in a synthesized one-dimensional (1D) temporal photonic system. The distribution of the beads (photons) at the bottom of the PGB corresponds to the shape of the generated arbitrary waveform, which is defined by the megahertz control signals applied to the AOMs. The key advantage of the proposed system is that low-speed control signals applied to the AOMs can make the PGB generate high-speed arbitrary waveforms with ultimate flexibility. The sampling rate of a generated arbitrary waveform can be continuously tuned by tuning the time delay difference between the two coupled loops to less than 1 ps, making a generated arbitrary waveform with a sampling rate of up to 1.64 TSa/s, as well as a wide sampling-rate tunable range from 10.42 GSa/s to 1.64 TSa/s. Our proposed fully reconfigurable PGB operating in the temporal synthetic dimension breaks the speed limit in a physical system, bringing arbitrary waveform generation into the TSa/s regime. The concept of dimension conversion also offers possible solutions to various physical dimension-related problems, such as super-resolution imaging, high-resolution spectroscopy, and high-precision time measurement.

## Results

**Photonic Galton board**. A traditional Galton board has multiple rows of pegs equally separated by a given interval. When a bead reaches a peg, it will be bounced to the right or left with a fixed probability of 50%. At the bottom of the Galton board, a Gaussian distribution of the beads is produced. In a PGB, as shown in Fig. 1a, multiple pegs with each having a tunable coupling ratio are used to bounce a photon to the left or right. The time delays of the left and right paths are $T_1$ and $T_2$, respectively. After putting a bunch of photons from the top of the PGB, an arbitrary temporal distribution of the photons will be produced at the bottom which is a temporally sampled arbitrary waveform with its shape and sampling rate determined by the coupling ratio and time delay difference, $T_2$-$T_1$, respectively. Thus, the PGB subtly translates the challenge of implementing an AWG with an ultra-high sampling rate into a path length matching problem. Figure 1b shows a fiber-optic system consisting of two coupled fiber-optic loops with different loop lengths incorporating an AOM in each of the two loops for the implementation of the PGB in the temporal synthetic dimension. An ultra-short optical pulse containing multiple photons (beads) from a mode-locked laser (MLL) with a temporal width $d$ is inputted into the long loop (blue line) through an optical coupler (OC1). The photons are split into two parts by a beam splitter (BS), which has a fixed splitting ratio, but the joint operation of the BS and the AOMs corresponds to a tunable BS with a splitting ratio controlled by the gain and loss of the AOMs. Then, the two groups of photons, i.e., two optical pulses, return to the BS and are split into four parts corresponding to four optical pulses. As the seed pulse recirculates in the two loops of different lengths for multiple round trips, at the output of each loop, a sequence of pulses is generated. By detecting the optical pulse sequences from the two loops at a detection unit (DU) the temporal distribution of the photons is produced, which is a temporally sampled arbitrary waveform with its shape determined by the tunable coupling ratio during different round trips. The time interval between adjacent pulses in the generated waveform is the time delay difference between the two loops, so the challenge in implementing an AWG with a TSa/s is subtly solved by matching fiber-optic length at a precision of micrometers. For a waveform generated at sub-TSa/s, the DU can be implemented

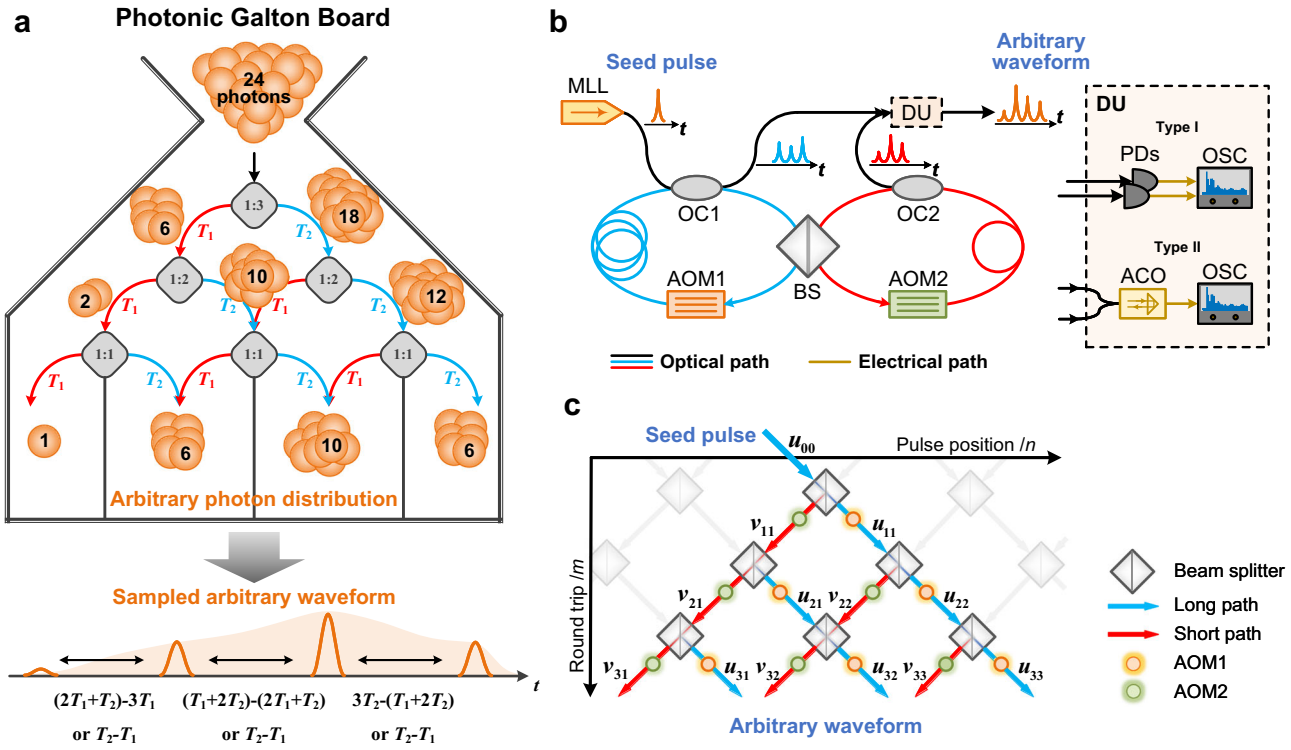


**Fig. 1 PGB in the temporal synthetic dimension. a** Photonic Galton board (PGB). The pegs (gray rounded rectangles) of each row have a tunable coupling ratio (the number in the gray rounded rectangles, corresponding to the coupling ratio), thus they can be made to control the number of photons (beads, orange circles) going to the left or right. $T_1$ and $T_2$ are the time delays of the left and right paths, respectively. At the bottom of the PGB, the temporal distribution of the photons is formed, which is a temporally sampled arbitrary waveform whose shape and sampling interval are determined by the pegs with tunable coupling ratio and path length difference, respectively. **b** The PGB implemented by fiber optics. An ultra-short optical pulse containing multiple photons from a mode-locked laser (MLL) is inputted into the long loop (blue line) through an optical coupler (OC1). The long loop and the short one (red line) are mutually coupled by a beam splitter (BS). Each loop contains an acousto-optic modulator (AOM1 or AOM2) for controlling the gain and loss of the optical pulses recirculating in the loops. After the seed pulse recirculates in the two loops for more round trips, a sequence of pulses is generated from each loop. By detecting and combining the optical pulse sequences at a detection unit (DU), a temporally sampled arbitrary waveform is generated. **c** Establishment of the temporal synthetic dimension. The blue and red arrowed lines indicate the pulses traveling in the long and short loops, respectively. The BS is depicted as a gray rectangle and the AOMs in the long and short loop are depicted as orange and green circles, respectively. The *n*-th pulse in the *m*-th round trip with an electric field $u_{m,n}$ in the long loop and $v_{m,n}$ in the short loop is coupled to its nearest neighbor sites $u(v)_{m+1,n+1}$ and $v(u)_{m+1,n}$ in the next round trip, respectively. As the pulses recirculate and couple in the two loops, a synthetic temporal dimension, pulse position *n*, is synthesized. PD photodetector, OSC oscilloscope, ACO optical autocorrelator.

by two photodetectors (PDs), of which the outputs are respectively sampled by two channels in a high-speed oscilloscope (OSC). For a waveform generated beyond TSa/s, the DU is implemented by directing the combined optical pulse sequences from the two loops to an optical autocorrelator (ACO), then the autocorrelation trace is sampled by a low-speed OSC. The equivalence of the fiber-optic system in Fig. 1b to a PGB is shown in Fig. 1c. The *n*-th pulse in the *m*-th round trip after being controlled by the AOM with an electric field $u_{m,n}$ in the long loop and $v_{m,n}$ in the short loop is coupled to its nearest neighbor sites $u(v)_{m+1,n+1}$ and $v(u)_{m+1,n}$ in the next round trip, respectively. As the pulses recirculate and couple in the two loops, a synthetic temporal dimension, pulse position *n*, is synthesized. We control the distributions of photons at different round trips at a speed of a few megahertz and tune the time delay difference between the two coupled loops with a time delay difference of less than 1 ps, an ultra-high speed arbitrary waveform at a TSa/s with ultimate flexibility is generated in the synthetic dimension. Thus, we successfully translate the speed and reconfigurability problems in a photonic AWG, where high-speed temporal manipulations are usually needed, to spatial length matching and low-speed acousto-optic modulation.

The electric field of the optical pulse at the output of the two loops can be expressed by

$$u_{m+1,n} = G_{u,m+1}\left(\frac{\sqrt{2}}{2}u_{m,n-1} + i\frac{\sqrt{2}}{2}v_{m,n}\right) \quad (1.1)$$

$$v_{m+1,n} = G_{v,m+1}\left(i\frac{\sqrt{2}}{2}u_{m,n-1} + \frac{\sqrt{2}}{2}v_{m,n}\right) \quad (1.2)$$

where $G_{u,m+1}$ and $G_{v,m+1}$ are the gain/loss of the AOMs in the long and short loop for the $(m+1)$-th round trip, respectively. As the seed pulse recirculates in the two loops of different lengths for more round trips, a temporally sampled arbitrary waveform $s[n]$ is generated at the bottom of the PGB. For a sub-TSa/s waveform detected by Type I DU, the waveform $s[n]$ achieved by combining the electrical pulse sequences after the PDs can be expressed by

$$s[n] = |u_{m,n}|^2 + |v_{m,n+1}|^2, 0 \le n \le m. \quad (2.1)$$

For a TSa/s waveform detected by Type II DU, the waveform $s[n]$ achieved by combining the optical pulse sequences from the

two loops before being sent to the ACO can be expressed by

$$s[n] = \left|\frac{\sqrt{2}}{2}u_{m,n} + i\frac{\sqrt{2}}{2}v_{m,n+1}\right|^2, 0 \le n \le m. \quad (2.2)$$

Equations (2.1) and (2.2) are initialized and ended with $u_{m,0} = 0$ and $v_{m,m+1} = 0$ (see Supplementary Note 1). The sampling interval of the generated waveform is equal to the time delay difference between the two loops which can be made ultra-small. The smallest sampling interval is only limited by the temporal width of the recirculating pulse at the $m$-th round trip, which will be broadened by the chromatic dispersion in the loops and is given by

$$d' = d + D \times \Delta\lambda \times m \times l \quad (3)$$

where $d$ is the temporal width of the seed pulse, $D$ is the dispersion coefficient of the loops, $\Delta\lambda$ is the spectrum width of the seed pulse, and $l$ is the length of the long loop. Thus, the sampling rate $f_s$ of the generated temporally sampled waveform can be expressed by

$$f_s = \frac{1}{T_2 - T_1} = \frac{1}{\Delta t} \le \frac{1}{d'} \quad (4)$$

where $\Delta t = T_2 - T_1$ is the time delay difference between the two loops. Equation (4) indicates that the sampling rate of the generated waveform from the PGB can be ultra-high when the time delay difference is ultra-small, and in this case, the maximum sampling rate is only limited by the temporal width of the recirculating pulse.

**Tera-sample-per-second arbitrary waveforms**. To experimentally evaluate the operation of the proposed PGB, the fiber-optic system in Fig. 1b is implemented (see Methods, and Supplementary Note 2). An optical pulse with a full width at half maximum (FWHM) of 460 fs is injected into the long loop as a seed pulse. In the short loop, we keep $G_{v,m} = 0.5$ by fixing the driving signal applied to AOM2 to be a sinusoidal signal at 200 MHz with a fixed amplitude. A second sinusoidal signal with a frequency of 80 MHz is amplitude modulated by $G_{u,m}$ at a symbol rate of 5.78 MHz. Then the modulated sinusoidal signal is applied to AOM1 as the control signal in the long loop. The different $G_{u,m}$ for the generation of different target waveforms are calculated by an *Auto-Fit* system with a backpropagation algorithm (see Supplementary Note 3). After the seed pulse recirculates in the PGB for 10 round trips, depending on the different control signals applied to AOM1, six different waveforms with 11 sampling points and different sampling rates are experimentally generated, which are shown in Fig. 2a–f. The dashed orange lines and solid blue lines show the target waveforms and the experimentally generated waveforms, respectively. Each orange dot is a sampling point in the target waveform. Two different waveforms with 31 sampling points and different sampling rates are also experimentally generated, as shown in Fig. 2g–j. By tuning the time delay difference between the two loops from 46.08 to 12.50 ps, the sampling rates of the generated waveforms can be arbitrarily controlled from 21.7 to 80.0 GSa/s. The average RMSE of the generated waveforms in Fig. 2 is calculated to be as small as 0.0741, confirming the good fidelity of the generated waveforms (see Supplementary Note 4).

To show the continuous tunability of the sampling rates, the evolutions of the 31-point Gaussian and rectangular waveforms when the time delay difference is continuously tuned from +100 to −100 ps are experimentally studied, as shown in Fig. 3. For the Gaussian waveform, the two dashed white lines in Fig. 3a indicate the variation in the sampling rate. During the continuous tunning of the time delay difference, the long loop will become a short loop if the time delay difference becomes negative. The corresponding sampling rate is increased from 10.00 GSa/s to infinity and then decreased from infinity back to 10.00 GSa/s. At the area near the intersections of the two dashed white lines, where the time delay difference is reduced to 1 ps or less, the sampling rate reaches a TSa/s or higher. Figure 3b shows the evolution of the generated Gaussian waveform in Fig. 3a plotted in 3D, where fifteen Gaussian waveforms with different sampling rates are shown. Figure 3c shows an experimentally generated Gaussian waveform in a blue line at 10.42 GSa/s. A target waveform in orange lines is also shown for comparison. A zoom-in view of an individual pulse in the target waveform is given in the inset by which the FWHM is measured to be 23.8 ps. Figure 3d shows an experimentally generated Gaussian waveform in a blue line at 341.56 GSa/s. The orange line shows the target waveform. Each orange dot is a sampling point of the target waveform. The generation of a rectangular waveform with 31 sampling points at different sampling rates is also performed and the results are shown in Fig. 3e–h. These experimental results are all achieved by using PDs with bandwidths of 50 GHz and a high-speed OSC with a bandwidth of 80 GHz, a sampling rate of 256 GSa/s, and a minimum rise/fall time of 5.6 ps (10–90%).

Due to the limited bandwidths of the PDs and the OSC, Type I DU can only sample a waveform at a sampling rate of less than a few hundred GSa/s. To evaluate a generated waveform beyond TSa/s, an ACO-based Type II DU is used to sample the ultrafast optical waveforms (see Supplementary Note 2). The autocorrelation traces of the generated arbitrary waveforms when the time delay difference is further tuned to less than 1 ps are shown as the blue lines in Fig. 4. The calculated autocorrelation traces of the target waveforms are also shown as yellow lines and dots for comparison. In Fig. 4a–c, the temporal interval between two adjacent autocorrelation points is 0.394 ms, corresponding to a sampling interval of 611 fs or an ultra-high sampling rate of 1.64 TSa/s in the generated waveforms, which are shown as the orange lines in the inserts (see Supplementary Note 5). Each orange dot in the inserts is a sampling point in the generated waveform. Based on the Nyquist sampling theorem, the sampling rate of 1.64 TSa/s results in a maximum bandwidth of 0.82 THz, the half of the sampling rate. The spectra of the generated triangular, rectangular, and sawtooth waveforms with a sampling rate of 1.64 TSa/s are shown in Fig. 4d–f, respectively, where 3-dB bandwidths of up to 250.3 GHz are achieved. Figure 4g, h show the generated Gaussian and 31-point rectangular waveforms with a sampling rate of 1.64 TSa/s. The spectra are also shown in Fig. 4i, j. Note that the bandwidth of the generated waveform is not as large as the maximum achievable bandwidth, due to the generated waveforms are not ultra-wideband signals. Furthermore, the sampling rate of a generated arbitrary waveform was determined by the time delay difference, which could be ultra-high, but is limited by the temporal width of the seed pulse and the dispersion in the two loops. In the experiment, although dispersion compensation was employed to eliminate the dispersion in the two loops, the pulses recirculating in the two loops may still be broadened due to residual dispersion, which made the sampling rate limited.

## Discussion

In conclusion, we have proposed and experimentally demonstrated a fully reconfigurable PGB in the temporal synthetic dimension, in which the temporal high-speed challenge was subtly translated into a spatial fiber-optic length matching problem, leading to the experimental generation of ultimately flexible arbitrary waveforms with widely and continuously tunable sampling rates from 10.42 GSa/s to 1.64 TSa/s. The PGB was

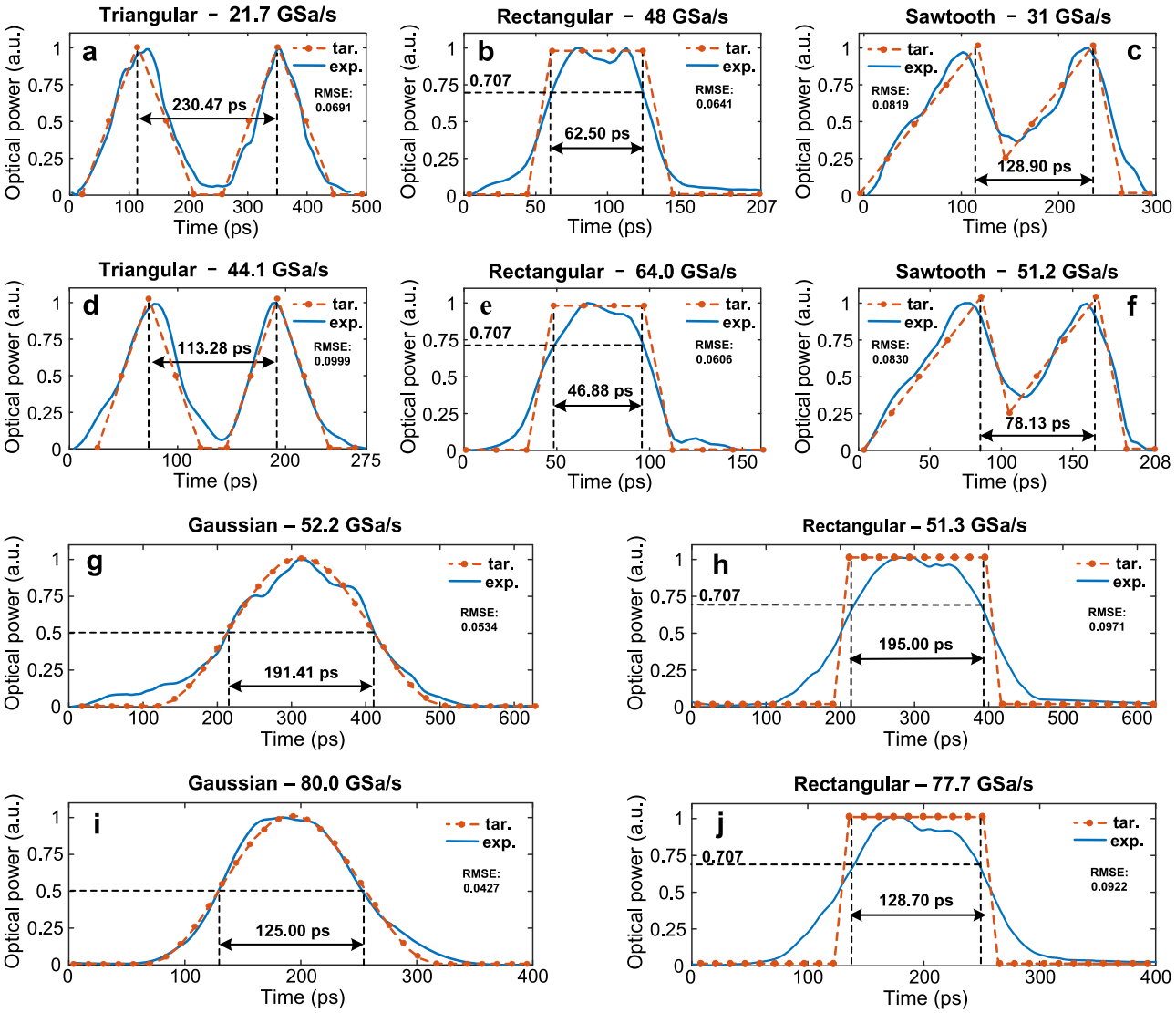


**Fig. 2 Experimentally generated arbitrary waveforms.** The generated waveforms (solid blue lines) with 11 sampling points at different sampling rates: **a** triangular at 21.7 GSa/s, **b** rectangular at 48.0 GSa/s, **c** sawtooth waveforms at 31.0 GSa/s, **d** triangular at 44.1 GSa/s, **e** rectangular at 64.0 GSa/s, and **f** sawtooth waveforms at 51.2 GSa/s. The generated waveforms with 31 sampling points: **g** Gaussian at 52.2 GSa/s, **h** rectangular at 51.3 GSa/s, **i** Gaussian at 80.0 GSa/s, and **j** rectangular at 77.7 GSa/s. The target waveforms are also shown as dashed orange lines for comparison. Each orange dot is a sampling point of the target waveform. The average RMSE is calculated to be 0.0741.

implemented in an all-fiber-based system, consisting of two coupled fiber-optic loops with different time delays. An AOM was incorporated in each loop to control the gain or loss of the optical pulse recirculating in the loop. At the bottom of the PGB, an arbitrary distribution of photons corresponding to the arbitrary waveform was generated. The shape of an arbitrary waveform was defined by the control signals applied to the AOMs, which made the PGB fully reconfigurable with ultimate flexibility. In comparison with the state-of-the-art electronic AWGs[32], our proposed PGB in the synthetic dimension has the same flexibility in arbitrary waveform generation, but it pushes the sampling rate into the TSa/s regime with a wider and continuous tunability. Compared with the AWGs based on optical pulse shaping in free space using pre-designed metasurfaces[35–38], the PGB was implemented in fiber optics, making it have a smaller size at a lower cost. Our proposed PGB also breaks the bandwidth limitations of the optical and optoelectronic components in fiber-optics-based pulse shaping systems[30,45,46,49,50], such as arrayed waveguide gratings, electro-optical modulators, and waveshapers. The PGB has the potential to be photonic integrated to further reduce the size and improve the stability for commercial applications[40,48,51–53].

In this paper, we showed that the photonic synthetic dimension can transform technical problems in photonic systems between dimensionalities, providing unexpected solutions to temporal high-speed problems that are otherwise challenging. The concept of dimension conversion offers possible solutions to various physical dimension-related problems, such as high-precision time measurement, high-resolution spectroscopy, super-resolution imaging, etc. By translating the temporal interval, spectral component, and space distance problem into the other dimensions or axes in a physical system, many ultimate technical issues may be subtly solved and profoundly pushed to new horizons.

## Methods

**The implementation of the PGB**. The PGB in the temporal synthetic dimension for the generation of ultra-high speed

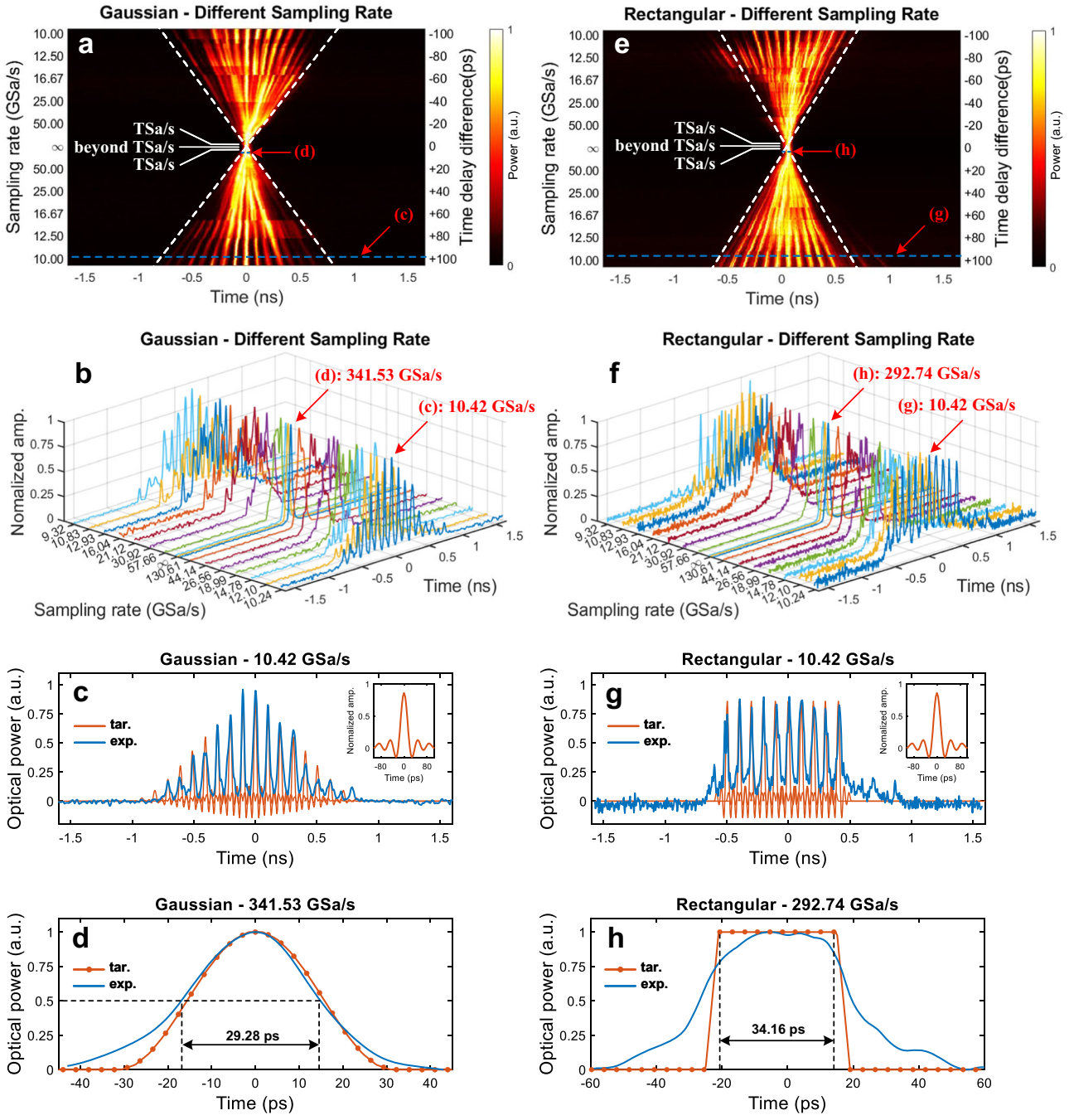


**Fig. 3 Continuous tuning of the sampling rate. a** The evolution of an experimentally generated Gaussian waveform when the time delay difference between the two loops is tuned from +100 to −100 ps. The dashed white lines show the evolution of the waveform width to indicate the variation in the sampling rate. At the area near the intersection of the two dashed white lines, the sampling rate can reach a TSa/s or higher when the time delay difference is within +1 and −1 ps. **b** The evolution of the generated Gaussian waveform shown in 3D. **c** A generated Gaussian waveform in solid blue lines at 10.42 GSa/s. A zoom-in view of an individual pulse in the target waveform is given in the inset which has a measured FWHM of 23.8 ps. **d** A generated Gaussian waveform in a solid blue line at 341.56 GSa/s. In **c** and **d**, the target waveforms in the orange lines are shown for comparison. Each orange dot is a sampling point of the target waveform. **e**–**h** show the generation of a rectangular waveform at different sampling rates.

arbitrary waveforms is implemented using commercial off-the-shelf optical and optoelectronic components (see Supplementary Note 2). An optical pulse train with a repetition rate of 20 MHz is generated by a femtosecond laser source (CALMAR OPTCOM FPL-03CFFJNU). Before being injected into the dual-loop fiber optic system, the repetition rate of the pulse train is reduced to 50 kHz through a Mach-Zehnder modulator (MZM, FUJITSU H74M-5208-J048) to make two adjacent pulses in the pulse train to have sufficiently large time spacing, so that a pulse can recirculate in the loops for multiple times without overlapping with a second pulse from the pulse train. The square signal applied to the MZM for selecting the seed pulse is generated by a two-channel AWG (RIGOL DG822). Then the seed pulse is injected into the long loop through OC1.

In the long loop, a tunable delay line (TDL, General Photonics MDL-002) with a maximum time delay of 560 ps and a time resolution of 1 fs is employed for controlling the time delay difference between the two loops, which enables the sampling rate of the

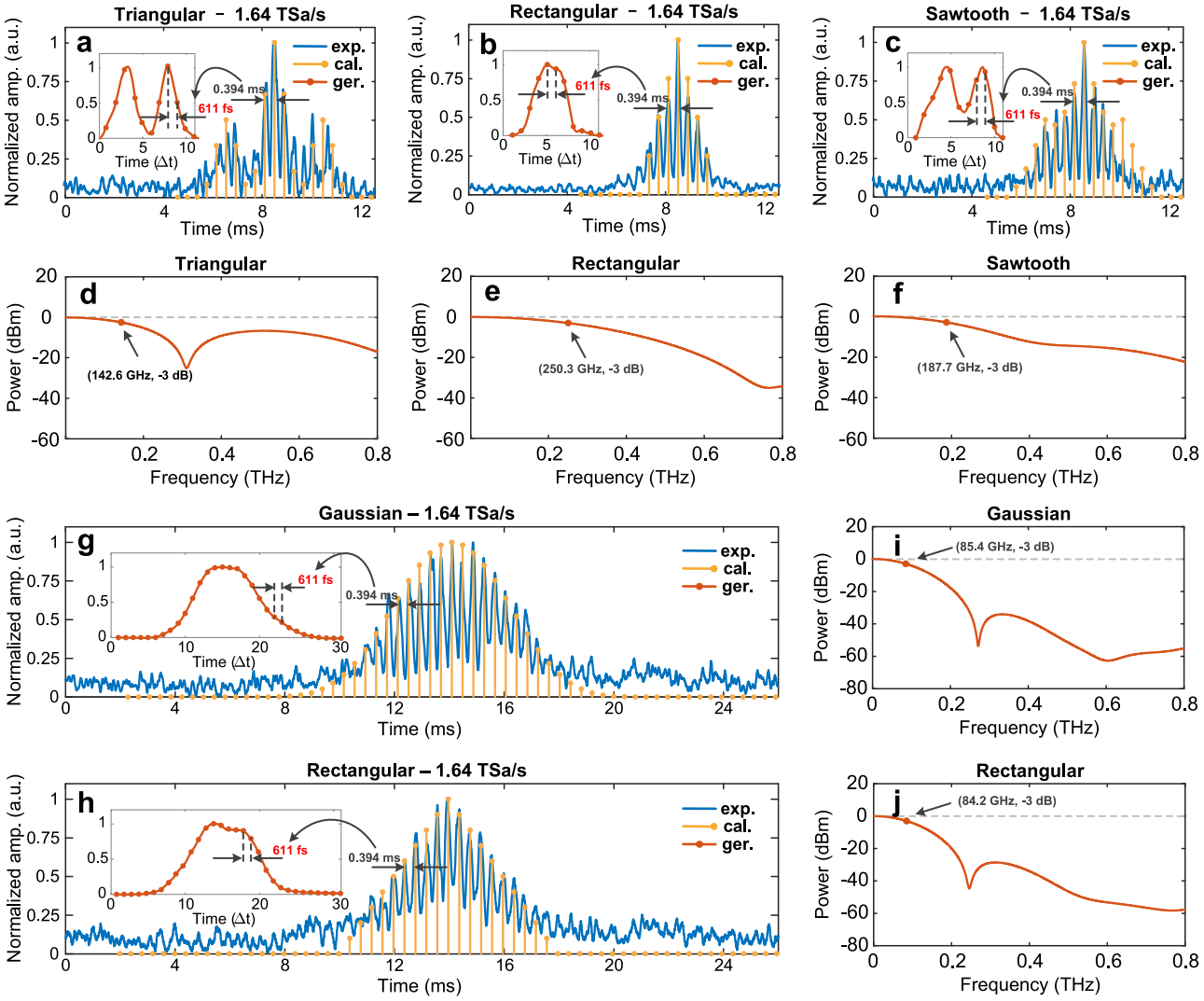


**Fig. 4 Experimentally generated 1.64 TSa/s arbitrary waveforms.** The blue lines show the autocorrelation traces of the generated (**a**) triangular, (**b**) rectangular, and (**c**) sawtooth waveforms. The temporal interval between two adjacent autocorrelation points is 0.394 ms, which corresponds to sampling intervals of 611 fs and sampling rates of 1.64 TSa/s in the generated waveforms, shown as the orange lines in the inserts. The calculated autocorrelation traces of the target waveforms are shown as yellow lines. The spectra of the target triangular, rectangular, and sawtooth waveforms with sampling rates of 1.64 TSa/s are shown in **d**, **e**, and **f**, respectively, which show 3-dB bandwidths of up to 250.3 GHz. The autocorrelation traces of the Gaussian and 31-point rectangular waveform are also shown in **g** and **h**. The corresponding spectra are shown in **i** and **j**, respectively.

generated arbitrary waveform can be continuously tuned with precision from 12.8 kSa/s @ 3.57 GSa/s to 1 GSa/s @ 1 TSa/s. An erbium-doped fiber amplifier (EDFA) and a tunable optical filter (TOF) are incorporated in each loop to ensure the seed pulse recirculates in the system for a sufficiently large number of round trips and to maintain a high signal-to-noise-ratio (SNR). To eliminate the chromatic dispersion in the two loops, a dispersion compensating fiber (DCF) of about 7 m is also employed in each loop. In the long loop, AOM1 (CETC SGTF80-1550-1) with a shifting frequency of 80 MHz, an EDFA (EDFA1, Max-Ray Photonics EDFA-BA-20-B) bumped at about 75 mA, and a TOF (TOF1, Santec OTF-350) with a center wavelength of 1553.11 nm and a passband of 4.94 nm are incorporated. In the short loop, AOM2 (Brimrose TEM-210-50-10-1550-2FP) has a shifting frequency of 200 MHz, the EDFA (EDFA2, PYOE-EDFA-C) is bumped at about 66 mA, and the TOF (TOF2, Alnair Labs BVF-300CL) is also working at a center wavelength of 1553.11 nm and a passband of 4.94 nm. Two polarization controllers (PCs) are also connected before the AOMs (AOM1 and AOM2) to minimize polarization-dependent loss. We adjust conjunctly the PC, EDFA, and TOF in each loop to ensure the seed pulse recirculates in each loop for a sufficiently large number of round trips, so that a predefined arbitrary waveform can be generated with a high SNR. After multiple round trips, OC1 and OC2 in each loop direct the pulse sequence to a detection unit (DU). For the waveforms at a speed of sub-TSa/s, the pulse sequence at the $10^{th}$ or the $30^{th}$ round trip is selected by an AOM (AOM3 or AOM4) and is detected by a PD (PD1 or PD2, $u^2t$ XPDV21x0RA) and sampled by two channels of a high-speed OSC (Keysight UXR 0804A) in the DU. If a generated waveform has sampling rate beyond TSa/s, the pulse sequences from the two loops are combined in another OC. Then, the pulse sequence at the $10^{th}$ or the $30^{th}$ round trip is selected by AOM3 and directed to the ACO. At the output of the ACO, the autocorrelation trace is displayed on a low-speed OSC (ATTEN ADS1302CE).

**The generation of arbitrary waveforms**. In the experiments, the PD has a bandwidth of 50 GHz. The high-speed OSC (Keysight UXR 0804A) has a bandwidth of 80 GHz, a sampling rate of 256 GSa/s, and a minimum rise/fall time of 5.6 ps (10–90%). The

autocorrelator (Femtochrome Research FR-103XL) has a delay calibration factor of 31 ps/ms @ 10 Hz. The autocorrelation trace displays dips between pulses or pulse sequences with repetition rates of less than 1 MHz (see Supplementary Note 5)[56]. The low-speed OSC (ATTEN ADS1302CE) has a bandwidth of 300 MHz and a sampling rate of 2 GSa/s. The square signal applied to the AOMs in the DUs is generated by the AWG (RIGOL DG822). The control signal applied to AOM1 in the long loop is generated by another AWG (Tektronix AWG70002A). The Sync port of the MLL is connected to the Trigger port of RIGOL DG822 for time synchronization. The Sync port of RIGOL DG822 is also connected to the Trigger port of Tektronix AWG70002A for time synchronization.

## Data availability

All the data supporting the findings of this study are available from the corresponding authors upon request.

Received: 25 June 2023; Accepted: 8 September 2023;
Published online: 19 September 2023

## References

1. Boada, O., Celi, A., Latorre, J. I. & Lewenstein, M. Quantum simulation of an extra dimension. *Phys. Rev. Lett.* **108**, 133001 (2012).
2. Mancini, M. et al. Observation of chiral edge states with neutral fermions in synthetic Hall ribbons. *Science* **349**, 1510–1513 (2015).
3. Yuan, L., Lin, Q., Xiao, M. & Fan, S. Synthetic dimension in photonics. *Optica* **5**, 1396–1405 (2018).
4. Lustig, E. et al. Photonic topological insulator in synthetic dimensions. *Nature* **567**, 356–360 (2019).
5. Li, G. et al. Dynamic band structure measurement in the synthetic space. *Sci. Adv.* **7**, eabe4335 (2021).
6. Qin, C. et al. Spectrum control through discrete frequency diffraction in the presence of photonic gauge potentials. *Phys. Rev. Lett.* **120**, 133901 (2018).
7. Buddhiraju, S., Dutt, A., Minkov, M., Williamson, I. A. & Fan, S. Arbitrary linear transformations for photons in the frequency synthetic dimension. *Nat. Commun.* **12**, 2401 (2021).
8. Ouyang, X. et al. Synthetic helical dichroism for six-dimensional optical orbital angular momentum multiplexing. *Nat. Photon.* **15**, 901–907 (2021).
9. Luo, X., Zhang, C., Guo, G. & Zhou, Z. Topological photonic orbital-angular-momentum switch. *Phys. Rev. A* **97**, 043841 (2018).
10. Weidemann, S. et al. Topological funneling of light. *Science* **368**, 311–314 (2020).
11. Wimmer, M., Monika, M., Carusotto, I., Peschel, U. & Price, H. M. Superfluidity of light and its breakdown in optical mesh lattices. *Phys. Rev. Lett.* **127**, 163901 (2021).
12. Bartlett, B., Dutt, A. & Fan, S. Deterministic photonic quantum computation in a synthetic time dimension. *Optica* **8**, 1515–1523 (2021).
13. Schreiber, A. et al. A 2D quantum walk simulation of two-particle dynamics. *Science* **336**, 55–58 (2012).
14. Wimmer, M., Price, H. M., Carusotto, I. & Peschel, U. Experimental measurement of the Berry curvature from anomalous transport. *Nat. Phys.* **13**, 545–550 (2017).
15. Li, L. et al. Polarimetric parity-time symmetry in a photonic system. *Light Sci. Appl.* **9**, 169 (2020).
16. Zhang, J. et al. Parity-time symmetry in wavelength space within a single spatial resonator. *Nat. Commun.* **11**, 3217 (2020).
17. Chalabi, H. et al. Synthetic gauge field for two-dimensional time-multiplexed quantum random walks. *Phys. Rev. Lett.* **123**, 150503 (2019).
18. Xiao, L. et al. Non-Hermitian bulk–boundary correspondence in quantum dynamics. *Nat. Phys.* **16**, 761–766 (2020).
19. Ozawa, T. & Price, H. M. Topological quantum matter in synthetic dimensions. *Nat. Rev. Phys.* **1**, 349–357 (2019).
20. Lustig, E. & Segev, M. Topological photonics in synthetic dimensions. *Adv. Opt. Photonics* **13**, 426–461 (2021).
21. Leefmans, C. et al. Topological dissipation in a time-multiplexed photonic resonator network. *Nat. Phys.* **18**, 442–449 (2022).
22. Regensburger, A. et al. Parity-time synthetic photonic lattices. *Nature* **488**, 167–171 (2012).
23. Wimmer, M. et al. Observation of optical solitons in PT-symmetric lattices. *Nat. Commun.* **6**, 7782 (2015).
24. Bouwmeester, D., Marzoli, I., Karman, G. P., Schleich, W. & Woerdman, J. P. Optical Galton board. *Phys. Rev. A* **61**, 013410 (1999).
25. Navarrete-Benlloch, C., Pérez, A. & Roldán, E. Nonlinear optical Galton board. *Phys. Rev. A* **75**, 062333 (2007).
26. Di Molfetta, G., Debbasch, F. & Brachet, M. Nonlinear optical Galton board: Thermalization and continuous limit. *Phys. Rev. E* **92**, 042923 (2015).
27. Gerasimenko, Y., Tarasinski, B. & Beenakker, C. W. J. Attractor-repeller pair of topological zero modes in a nonlinear quantum walk. *Phys. Rev. A* **93**, 022329 (2016).
28. Yao, J. P. Arbitrary waveform generation. *Nat. Photon.* **4**, 79–80 (2010).
29. Cundiff, S. T. & Weiner, A. M. Optical arbitrary waveform generation. *Nat. Photon.* **4**, 760–766 (2010).
30. Yao, J. P. Photonic generation of microwave arbitrary waveforms. *Opt. Commun.* **284**, 3723–3736 (2011).
31. Rashidinejad, A., Li, Y. & Weiner, A. M. Recent advances in programmable photonic-assisted ultrabroadband radio-frequency arbitrary waveform generation. *IEEE J. Quantum Electron* **52**, 1–17 (2016).
32. Keysight M8199A *Arbitrary Waveform Generator*, https://www.keysight.com/us/en/product/M8199A/arbitrary-waveform-generator-128-256-gsas.html (2023).
33. Ferdous, F. et al. Spectral line-by-line pulse shaping of on-chip microresonator frequency combs. *Nat. Photon* **5**, 770–776 (2011).
34. Weiner, A. M. Femtosecond pulse shaping using spatial light modulators. *Rev. Sci. Instrum.* **71**, 1929–1960 (2000).
35. Veli, M. et al. Terahertz pulse shaping using diffractive surfaces. *Nat. Commun.* **12**, 37 (2021).
36. Divitt, S., Zhu, W., Zhang, C., Lezec, J. H. & Agrawal, A. Ultrafast optical pulse shaping using dielectric metasurfaces. *Science* **364**, 890–894 (2019).
37. McKinney, J. D., Leaird, D. E. & Weiner, A. M. Millimeter-wave arbitrary waveform generation with a direct space-to-time pulse shaper. *Opt. Lett.* **27**, 1345–1347 (2002).
38. Maroju, P. K. et al. Attosecond pulse shaping using a seeded free-electron laser. *Nature* **578**, 386–391 (2020).
39. Yao, J. P. Microwave photonics. *J. Lightw. Technol.* **27**, 314–335 (2009).
40. Marpaung, D., Yao, J. P. & Capmany, J. Integrated microwave photonics. *Nat. Photon.* **13**, 80–90 (2019).
41. Zou, X. et al. Photonics for microwave measurements. *Laser Photonics Rev.* **10**, 711–734 (2016).
42. Okada, T., Kobayashi, R., Rui, W., Sagara, M. & Matsuura, M. Photonic digital-to-analog conversion using a blue frequency chirp in a semiconductor optical amplifier. *Opt. Lett.* **45**, 1483–1486 (2020).
43. Zhang, J. & Yao, J. P. Time-stretched sampling of a fast microwave waveform based on the repetitive use of a linearly chirped fiber Bragg grating in a dispersive loop. *Optica* **1**, 64–69 (2014).
44. Meng, J., Miscuglio, M., George, J. K., Babakhani, A. & Sorger, V. J. Electronic bottleneck suppression in next-generation networks with integrated photonic digital-to-analog converters. *Adv. Photon Res.* **2**, 2000033 (2020).
45. Chi, H., Wang, C. & Yao, J. P. Photonic generation of wideband chirped microwave waveforms. *IEEE J. Microwav.* **1**, 787–803 (2021).
46. Xie, Q., Zhang, H. & Shu, C. Programmable schemes on temporal waveform processing of optical pulse trains. *J. Lightw. Technol.* **38**, 339–345 (2020).
47. Zhang, J. & Yao, J. P. Parity-time-symmetric optoelectronic oscillator. *Sci. Adv.* **4**, eaar6782 (2018).
48. Hao, T. et al. Breaking the limitation of mode building time in an optoelectronic oscillator. *Nat. Commun.* **9**, 1839 (2018).
49. Tang, J. et al. Hybrid Fourier-domain mode-locked laser for ultra-wideband linearly chirped microwave waveform generation. *Nat. Commun.* **11**, 3814 (2020).
50. Tan, M. et al. Photonic RF arbitrary waveform generator based on a soliton crystal micro-comb source. *J. Lightw. Technol.* **38**, 6221–6226 (2020).
51. Liu, W. et al. An integrated parity-time symmetric wavelength-tunable single-mode microring laser. *Nat. Commun.* **8**, 15389 (2017).
52. Liu, W. et al. A fully reconfigurable photonic integrated signal processor. *Nat. Photon.* **10**, 190–195 (2016).
53. Liu, J. et al. Photonic microwave generation in the X-and K-band using integrated soliton microcombs. *Nat. Photon* **14**, 486–491 (2020).
54. Zhang, W. & Yao, J. P. A fully reconfigurable waveguide Bragg grating for programmable photonic signal processing. *Nat. Commun.* **9**, 1396 (2018).
55. Zhang, W. & Yao, J. P. Photonic integrated field-programmable disk array signal processor. *Nat. Commun.* **11**, 406 (2020).
56. Yasa, Z. A. & Amer, N. M. A rapid-scanning autocorrelation scheme for continuous monitoring of picosecond laser pulses. *Opt. Commun.* **36**, 406–408 (1981).

## Acknowledgements

Guangdong Province Key Field R&D Program Project (2020B0101110002); National Key Research and Development Program of China (2021YFB2800804); Guangdong

Engineering Technology Research Center for Integrated Space-Terrestrial Wireless Optical Communication.

## Author contributions

Y.G. and J.Z. conceived the idea, designed the experiment, and analyzed the data; Y.G. and L.L. performed the experiment; R. C., G. W., and J. C. contributed to the experiment; Y.G. wrote the paper; J.Z., X.W., and J.Y. revised the paper; J.Z., B-O. G., X.W., and J.Y. administrated the project and supervised the work.

## Competing interests

The authors declare no competing interests.

## Additional information

**Supplementary information** The online version contains supplementary material available at https://doi.org/10.1038/s42005-023-01383-x.

**Correspondence** and requests for materials should be addressed to Jiejun Zhang or Jianping Yao.

**Peer review information** *Communications Physics* thanks the anonymous reviewers for their contribution to the peer review of this work.